POTENTIAL OF TUBULAR SOLAR STILL WITH RECTANGULAR TROUGH FOR WATER PRODUCTION UNDER VACUUM CONDITION

by

Mohamed Bechir BEN HAMIDA [a,b,c,d*], Fuhaid ALSHAMMARI[a], Ibrahim ALATAWI[a], Muapper ALHADRI[a], Mohammed A. ALMESHAAL[d], and Khalil HAJLAOUI[d]

[a]College of Engineering, Department of Chemical Engineering, University of Ha'il, Ha'il, Saudi Arabia
[b]Research Laboratory of Ionized Backgrounds and Reagents Studies (EMIR), Preparatory Institute for Engineering Studies of Monastir (IPEIM), University of Monastir, Monastir City, Tunisia
[c]Higher School of Sciences and Technology of Hammam Sousse, Department of Physics, University of Sousse, Sousse, Tunisia
[d]College of Engineering, Department of Mechanical Engineering, Imam Mohammad Ibn Saud Islamic University (IMSIU), Riyadh, Saudi Arabia

Original scientific paper
https://doi.org/10.2298/TSCI211116029B

Water scarcity, energy scarcity, and demographic difficulties are all real concerns for many countries throughout the world. Due to the high solar intensities and long sunshine duration in Saudi Arabia, solar water desalination can be effectively utilized for obtaining fresh water. The aim of this paper is explore the potential of simple-design and plentiful rectangular trough in desalination under vacuum condition. Numerical analysis of the heat and mass transfer of tubular solar still containing rectangular trough was performed. A 2-D code that solves the systems of equations for mass, momentum, concentration, and energy was developed and validated. The effect of the rib and the vertical elevation of the trough on heat and mass transfer were investigated. The numerical results showed that the distillation rate is significantly increased with the increase of the rib of the trough at a minimum of 19.78%. In addition, the distillation rate is increased at a minimum of 12.88% when the trough moves towards the upper side of the glass cover where the condensation takes place.

Keywords*: tubular solar still, rectangular trough, heat and mass transfer, vacuum condition, distillation rate, trough position, COMSOL multiphysics.*

Introduction

Water, like food and air, is a basic human need. The value of providing fresh water cannot be overstated. Many people, especially in arid regions and remote areas, have been affected by a lack of safe drinking water. Solar distillation would be an effective remedy for

*Corresponding author, e-mail: benhamida_mbechir@yahoo.fr

the lack of water supplies in these regions if they were rich in solar energy. Solar energy has been considered as one of the finest methods for powering the desalination procedure in arid places with abundant solar resources. Solar stills are the most often utilized solar desalination devices in rural places due to their ease of building and maintenance [1-5].

Despite various advancements in solar still shape, their low productivity remains the most fundamental drawback in their general use. As a result, more modern solar stills are being designed to optimize freshwater output.

A tubular solar still (TSS) is an ancient technique that uses the same distillation principle as a traditional basin solar still but is different in its cylindrical form. Many of the experimental and theoretical studies have been interested in solar distillation using TSS. Elashmawy and Alshammari [6] investigated the action of tubular stills containing calcium chloride as a desiccant material for collecting water from ambient air. They discovered that the distillation rate was 0.51 L per kilogram of calcium chloride. Kabeel *et al*. [7] used cover cooling technology to improve tubular still distillation rate. They discovered that using cooling technology increased distillation rate by 31.4%. Elashmawy [8] studied the influence of surface cooling and tube thickness on the performance of a high temperature solo TSS using empirical data. The effects of absorber surface shapes on tubular still distillation rate were investigated by Elshamy and El-Said [9]. They found that using a corrugated absorber surface improved distillation rate by 26.47%. The effects of the glass cover angle and the form of the absorber surface on the distillation rate of solar stills were investigated empirically by Goshayeshi and Safaei [10]. The effects of cover cooling on the action of tubular stills with CPC were studied by Arunkumar *et al*. [11]. Other previous studies have been conducted with the aim of improving solar still efficiency, either by improving the design of solar stills [12, 13] or by adding thermal storage materials [14, 15].

Another choice for improving the efficiency of solar stills is to run them in vacuum. According to Ahmed *et al*. [16], at 50 kPa, a three-stage solar still's freshwater supply might be enhanced by 45% compared to 101 kPa. Gude *et al*. [17] investigated a two-stage vacuum-operated still with a 60 °C heat source and found that the distillation efficiency was 1.5.

Despite of a few research works was carried out for the case of TSS operating with rectangular trough under vacuum condition [18-20], the influence of the variation of through position and its dimensions inside the tubular shell have not yet been studied. This is the objective of this study in particular with a rectangular trough having a square cross-section.

Physical Issue

The problem's geometry and description

Figure 1 presents the geometry of a simple effect TSS with rectangular trough which contains the seawater at the temperature, T_w, and the concentration of, C_w. The cover has a temperature of, T_s, which is always lower than the temperature of water. The rectangular trough placed in the center of the tubular shell of cylindrical shape, has a square cross section.

An external vacuum pump is utilized to empty the enclosure and maintain the chamber's vacuum during operation. As solar energy is absorbed, the saltwater in the rectangular trough continues to evaporate. Water vapor rises from the water surface due to buoyancy forces and condenses on the inner surface of the upper shell. The condensate trickles down the inner shell surface and gathers at the bottom of the still, where the fresh water is retrieved, due to gravity.

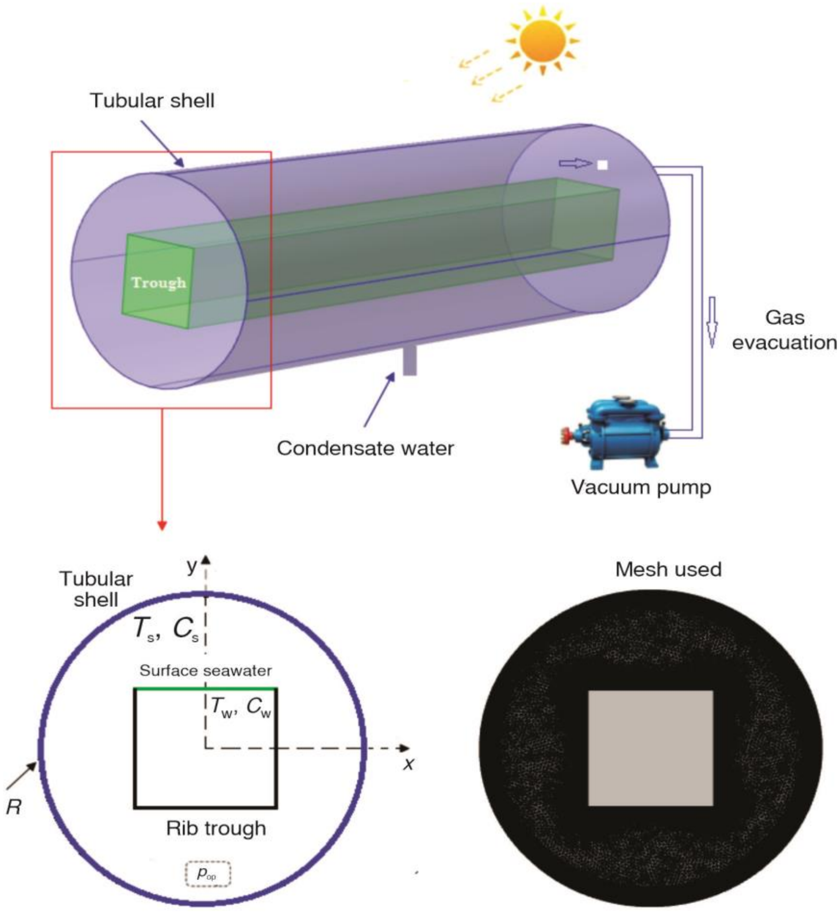

Figure 1. Schematic representation of the computational domain

Simplifying assumptions

The following assumptions about the operating parameters of TSS are established in order to study the thermal and flow properties of this 2-D model in unsteady-state:

– The fluid is a combination of water vapor and air that is incompressible and Newtonian.
– The fluid flow is 2-D and laminar.
– The temperatures of the water and cover are constant.
– The trough-wall is adiabatic.
– Heat transfer by radiation and viscous dissipation are negligible.

Governing equations

The unsteady-state governing equations for mass, momentum, concentration, and energy conservation are given.

Continuity equation:

$$\frac{\partial U}{\partial X}+\frac{\partial V}{\partial Y}=0 \tag{1}$$

The dimensionless velocity components according to the X and Y axes are U and V, respectively.

Momentum equation according to X axis:

$$\frac{\partial U}{\partial \tau}+U\frac{\partial U}{\partial X}+V\frac{\partial U}{\partial Y}=-\frac{\partial P}{\partial X}+\mathrm{Pr}\left(\frac{\partial^2 U}{\partial X^2}+\frac{\partial^2 U}{\partial Y^2}\right) \tag{2}$$

where Pr is the Prandtl number and τ and P are, respectively, the dimensionless time and pressure.

Momentum equation according to Y axis:

$$\frac{\partial V}{\partial \tau}+U\frac{\partial V}{\partial X}+V\frac{\partial V}{\partial Y}=-\frac{\partial P}{\partial Y}+\mathrm{Pr}\left(\frac{\partial^2 V}{\partial X^2}+\frac{\partial^2 V}{\partial Y^2}\right)+\mathrm{Ra_T}\,\mathrm{Pr}\left(\theta+BrC\right) \tag{3}$$

where $\mathrm{Ra_T}$ is the thermal Rayleigh number, Br – the buoyancy ratio, and θ and C are the dimensionless temperature and concentration, respectively.

Energy equation:

$$\frac{\partial \theta}{\partial \tau}+U\frac{\partial \theta}{\partial X}+V\frac{\partial \theta}{\partial Y}=\frac{\partial^2 \theta}{\partial X^2}+\frac{\partial^2 \theta}{\partial Y^2} \tag{4}$$

Concentration equation:

$$\frac{\partial C}{\partial \tau}+U\frac{\partial C}{\partial X}+V\frac{\partial C}{\partial Y}=\frac{1}{\mathrm{Le}}\left(\frac{\partial^2 C}{\partial X^2}+\frac{\partial^2 C}{\partial Y^2}\right) \tag{5}$$

where Le is the Lewis number.

The dimensionless variables are defined:

$$\begin{gathered}X=\frac{x}{R},\ Y=\frac{y}{R},\ U=\frac{uR}{\nu},\ V=\frac{vR}{\nu},\ \tau=\frac{t\alpha}{L^2},\ P=\frac{pR^2}{\rho\nu},\ \theta=\frac{T-T_\mathrm{s}}{T_\mathrm{w}-T_\mathrm{s}},\ C=\frac{c-c_\mathrm{s}}{c_\mathrm{w}-c_\mathrm{s}}\\ \mathrm{Pr}=\frac{\nu}{\alpha},\ \mathrm{Ra_T}=\frac{\mathrm{g}\beta_T\left(T_\mathrm{w}-T_\mathrm{s}\right)L_c^3}{\nu\alpha},\ Br=\frac{\beta_c\left(c_\mathrm{w}-c_\mathrm{s}\right)}{\beta_T\left(T_\mathrm{w}-T_\mathrm{s}\right)},\ \mathrm{Le}=\frac{\alpha}{D_{AB}}\end{gathered} \tag{6}$$

The average distance between the water's surface and the shell's inner surface is the characteristic length, L_c.

The coefficient for thermal expansion,β_T, is defined as [21]:

$$\beta_T=-\frac{1}{\rho}\frac{\partial \rho}{\partial T} \tag{7}$$

The coefficient for concentration expansion is defined as [22]:

$$\beta_c=-\frac{1}{\rho}\frac{\partial \rho}{\partial c}=\frac{1}{\rho}\left(\frac{M_\mathrm{a}}{M_\mathrm{w}}-1\right) \tag{8}$$

The mass diffusion coefficient was determined using [23]:

$$D_{AB}=\frac{\left(\dfrac{1}{M_A}+\dfrac{1}{M_B}\right)^{0.5}T^{1.75}}{p_\mathrm{op}\left[\left(\sum_A d_i\right)^{1/3}+\left(\sum_B d_i\right)^{1/3}\right]^2}\times 10^{-3} \tag{9}$$

For water and air, the diffusion volume, d_i, values were 12.7 cm^3/mol and 20.1 cm^3/mol, respectively [20].

The rate at which fresh water is produced, also known as productivity, m_{hourly}, was determined using [20]:

$$m_{\text{hourly}} = \frac{-3600 D_{AB}}{L_{\text{w}}} \int_0^{L_{\text{w}}} \left.\frac{\partial c}{\partial y}\right|_{y=0} \text{d}x \tag{10}$$

The average Nusselt number, $\overline{\text{Nu}}_{\text{w}}$, on the water surface was determined [20]:

$$\overline{\text{Nu}}_{\text{w}} = \frac{-L_{\text{c}}}{L_{\text{w}}\left(T_{\text{w}} - T_{\text{s}}\right)} \int_0^{L_{\text{w}}} \left.\frac{\partial T}{\partial y}\right|_{y=0} \text{d}x \tag{11}$$

where parameter L_{w} is the width of water surface.

Boundary conditions

The model's boundary conditions were reported in tab. 1.

Table 1. Boundary conditions for dimensionless form

Border	Condition on U	Condition on V	Condition on θ	Condition on C
Tubular shell	0	0	0	0
Seawater surface	0	0	1	1
Trough wall	0	0	$\frac{\partial \theta}{\partial n} = 0$	$\frac{\partial C}{\partial n} = 0$

Numerical method and validation

The flow structure inside the TSS was modelled using COMSOL Multiphysics 5.5. The decision was made to adopt a second-order upwind discretization method. The species transport model for the air-vapor mixture was enabled in the simulation. The density was set as an incompressible ideal gas, the specific heat capacity was estimated using the mixing law, and the thermal conductivity and viscosity were calculated using the mass weighted mixing law. When the scaled-residuals for the energy equation were less than 10^{-6} and 10^{-4} for the others, the solution was considered convergent.

To verify that the mesh of the TSS is appropriate for providing a valid result for heat transfer and flow characterisation, a grid independent test is carried out first.

Table 2. Initial parameters of TSS

Radius of tubular shell, R	0.8 m
Rib of square trough	60 mm
Operating pressure, p_{op}	101 kPa
Seawater temperature, T_{w}	60 °C
Thermal Rayleigh number, Ra_{T}	1.3 105
Buoyancy ratio, Br	2.4

Table 2 shows the initial validation requirements. In order for further mesh refinement to have no effect on the results, the percentage of variation of the analysis results must be less than 2%.

Table 3 summarizes the test results. Figure 2(a) shows the productivity and the average Nusselt number for varying mesh element numbers on the water surface. From both tab. 3 and fig. 2, it is clearly shown that the distillation rate and the average Nusselt number are constant from the last two meshes *i.e.* extra fine and extremely fine. The mesh used is extremely fine which contains 28636 elements and presented in fig. 1. An Intel(R) Core(TM) i7-4790 CPU at 3.60 GHz processor with 32 GB RAM has been used to perform the simulations.

Table 3. Mesh sensitivity

Type of mesh	Elements number of mesh	Distillation rate [kgm^{-2}hr^{-1}]	Nusselt number
Extremely coarse	389	0.3955	2.3877
Extra coarse	662	0.4237	2.5581
Coarser	912	0.4340	2.6206
Coarse	1626	0.4532	2.7361
Normal	2430	0.4755	2.7993
Fine	3776	0.5046	2.8709
Finer	9474	0.5260	3.0465
Extra Fine	24114	0.5263	3.1773
Extremely Fine	28636	0.5263	3.1773

This model is also used to validate with experimental work done by Elashamwy [24] on June 26, 2016 in Ha'il, KSA. According to the temporary temperature conditions of trough, inside tube surface and ambient. The evolution of the distillation rate for each hour of this day is calculated numerically by our code which is presented in fig. 2(b). From this figure, we see the good agreement between the numerical results found by our code and the experimental results carried out by Elashamawy [24].

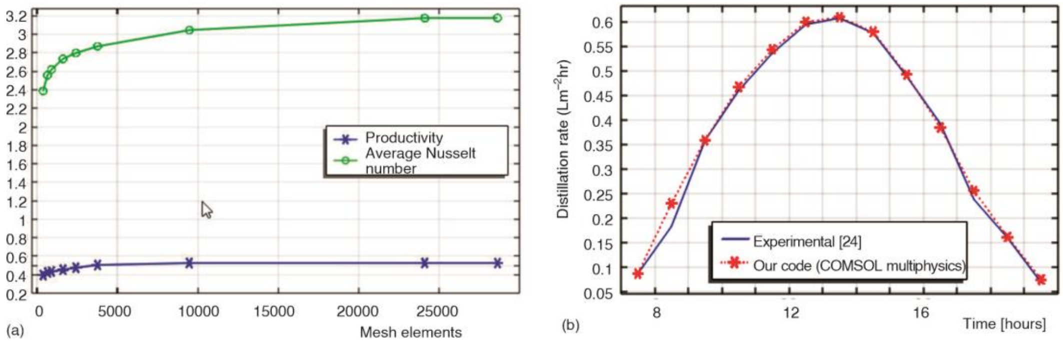

Figure 2. (a) Productivity and the average Nusselt number on the water surface for different elements number of mesh and (b) comparison of experimental and numerical distillation rate

Results and discussion

After the validation of our numerical code, it is used to study the effect of the rib and the vertical elevation of the square trough on the heat and mass transfer inside the TSS and especially the productivity of distillate water.

Effect of the rib of square trough

In this section, we deal to study the influence of the rib of the square trough on the heat and mass transfer inside the TSS. For this, we vary the rib of the square trough from 20 mm to 75 mm in the center of the tubular shell keeping the temperature of the glass cover, the initial seawater temperature, and the operating pressure illustrated in tab. 2 constant.

Figure 3 shows the contours of velocity for various ribs of the trough (20 mm, 30 mm, 40 mm, 50 mm, 60 mm, 70 mm, and 75 mm). From this figure, we see that the velocity decreases with the increase of the rib of the square trough. Indeed, for the rib of 20 mm, the maximum velocity is 0.36 m/s. But, in the case of 75 mm of the rib square of the trough, the velocity does not exceed 0.092 m/s. The maximum of velocity are 0.36 m/s; 0.33 m/s; 0.27 m/s; 0.23 m/s; 0.165 m/s; 0.115 m/s and 0.092 m/s which correspond respectively to the rib of the square trough 20 mm; 30 mm; 40 mm; 50 mm; 60 mm; 70 mm and 75 mm.

Figure 3 shows the contours of vorticity for different ribs of the trough (20 mm; 30 mm; 40 mm; 50 mm; 60 mm; 70 mm and 75 mm). From this figure, we see that found two cells between the square troughs. In addition, the vorticity increases significantly between the upper rib of the square and the upper tubular shell when the rib of the square trough increases.

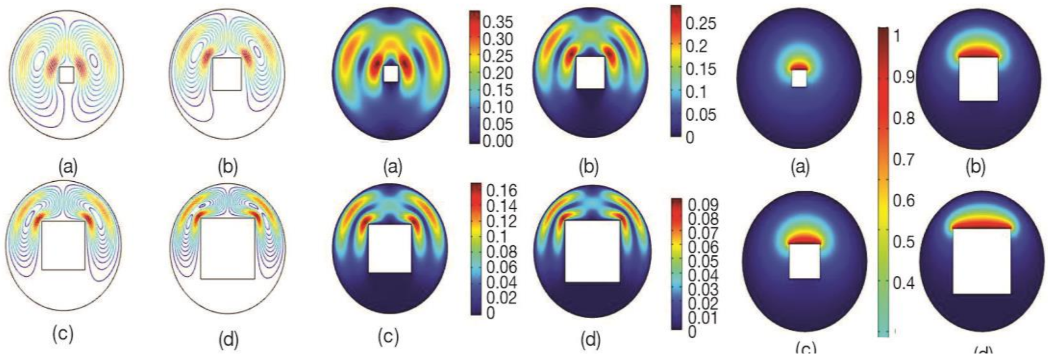

Figure 3. Contours of vorticity (left) velocity (middle), and temperature (right) for various ribs of trough at T_w=60 °C and p_{op} = 101 kPa; (a) 20 mm, (b) 40 mm, (c) 60 mm, and (d) 75 mm

Figure 3 shows the contours of temperature for several ribs of the trough (20 mm, 30 mm, 40 mm, 50 mm, 60 mm, 70 mm, and 75 mm). From this figure, it is clear that the hot zone is localized only between the upper face of the square trough and the upper surface of the tubular shell. This is due to the phase of the evaporation of the seawater. While the lower area is cold since it is the recovery area for distilled water after its condensation.

To study the effect of heat and mass transfer, we plot the Nusselt number according to each square rib of the trough (20 mm, 30 mm, 40 mm, 50 mm, 60 mm, 70 mm, and 75 mm) at T_w = 60 °C and p_{op} = 101 kPa shown in fig. 4. From this figure, we see that the Nusselt number increases when the rib of the square trough increases. Indeed, the Nusselt number is 1.26 when the rib of the square trough is 20 mm and reaches 3.08 for the case of 75 mm of rib square trough. In other words, the phenomenon of convection and conduction is almost proportional when the trough dimension is 20 mm. On the other hand, in the case where the dimension of trough increases the phenomenon of convection will be more important than the conduction and will be three times in where the dimension of the trough is 75 mm. This is explained by the narrowing of the distance between the hot zone and the cold zone during the increase of the trough dimension where the transfer by convection will be much significant.

To investigate the effect of distillation rate *i.e.* the productivity of distillate water of the TSS with square trough, we plot the distillation rate according to each square rib of the trough (20 mm, 30 mm, 40 mm, 50 mm, 60 mm, 70 mm, and 75 mm) at T_w = 60 °C and p_{op} = 101 kPa shown in fig. 3. From this figure, we observe that the productivity of distillate water increases with the increase of the rib of the square trough. Indeed, the distillation rate is 0.20899 kg/(m^{2}hr) for the case of the rib square trough is 20 mm. This quantity increase of 19.78%, 39.65%, 62%, 88.87%, 122.88%, and 144% when the rib of the square trough is 30 mm, 40 mm, 50 mm, 60 mm, 70 mm, and 75 mm, respectively. These results confirm the effect of convection and the Nusselt number seen in fig. 4. We conclude that the rib of the square trough is an important parameter for increasing the productivity of distillate water.

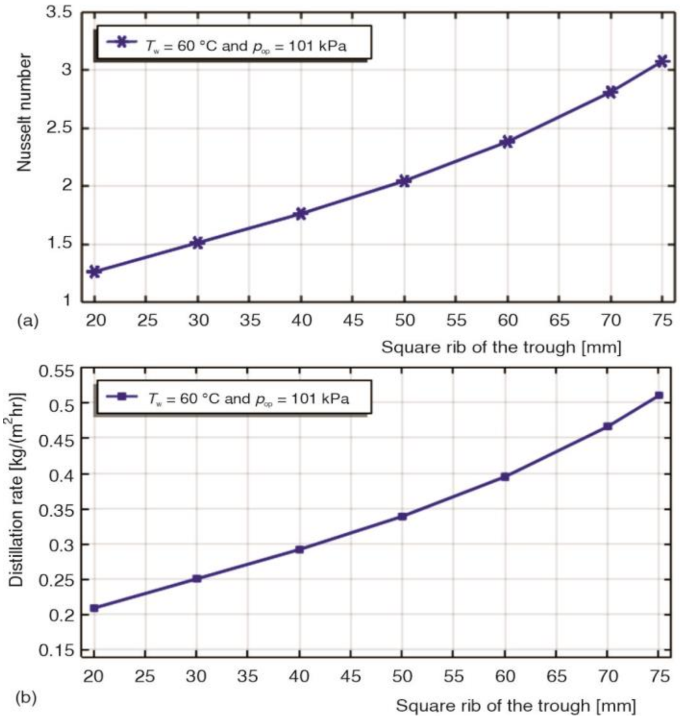

Figure 4. Evolution of (a) Nusselt number and (b) distillation rate according to square rib of the trough at T_w = 60 °C and p_{op} = 101 kPa

Effect of the vertical elevation of square trough

The aim of this section is to investigate the impact of the square trough's vertical elevation on heat and mass transfer within the TSS. Therefore, we shift vertically and upwards the through position of the middle of the tubular shell from 5 mm to 30 mm maintaining the temperature of the glass cover, the initial seawater temperature, and the operating pressure illustrated in tab. 2 are constant. Figures 5 and 6 show the contours of velocity of several square ribs of trough (*SR* = 0.02 m, 0.03 m, 0.04 m, 0.05 m, 0.06 m, 0.07 m, and 0.075 m) at T_w = 60 °C and p_{op} = 101 kPa for different vertical elevation of the trough (5 mm, 10 mm, 15 mm, 20 mm, 25 mm, and 30 mm).

From these figures, we see that the velocity decreases with the elevation position of the square trough from the center of the tubular shell to its upper surface. Indeed, when the square trough is in the middle of the tubular trough and its rib is 60 mm, the maximum velocity is 0.165 m/s. But, when it is elevated to the upper surface of 5 mm, 10 mm, 15 mm, 20 mm, 25 mm, and 30 mm, the maximum velocity decreases by 15.15%, 33.33%, 45.45%, 63.63%, 73.33%, and 82.85%, respectively.

Figures 7 and 8 show the contours of vorticity for different ribs of the trough (SR = 0.02 m, 0.03 m, 0.04 m, 0.05 m, 0.06 m, 0.07 m, and 0.075 m) at T_w = 60 °C and p_{op} = 101 kPa for different vertical elevation of the trough (5 mm, 10 mm, 15 mm, 20 mm, 25 mm, and 30 mm). From these figures, we can see that there are two cells between the square troughs. When the square trough moves up, the vorticity between the upper rib of the square and the upper tubular shell increases significantly and decreases in the lower area.

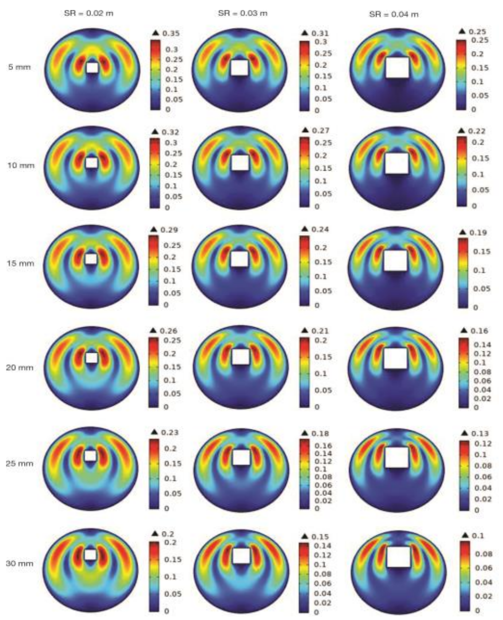

Figure 5. Contours of velocity of 3 various square ribs of trough (SR = 0.02 m, 0.03 m, and 0.04 m) at T_w = 60 °C and p_{op} = 101 kPa for different vertical elevation of the trough (5 mm, 10 mm, 15 mm, 20 mm, 25 mm, and 30 mm)

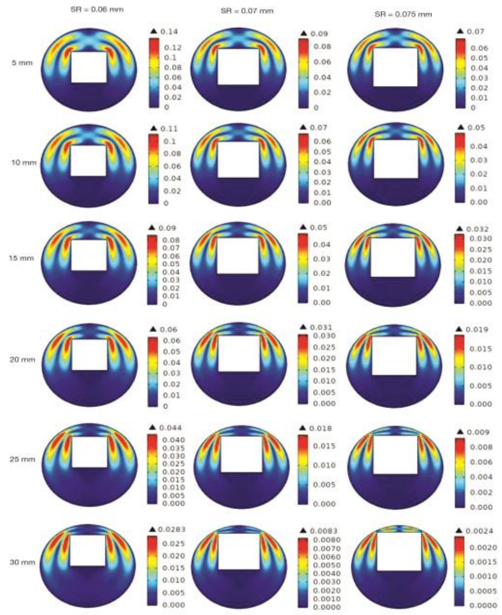

Figure 6. Contours of velocity of 3 various square ribs of trough (SR = 0.06 m, 0.07 m, and 0.075 m) at T_w = 60 °C and p_{op} = 101 kPa for different vertical elevation of the trough (5 mm, 10 mm, 15 mm, 20 mm, 25 mm, and 30 mm)

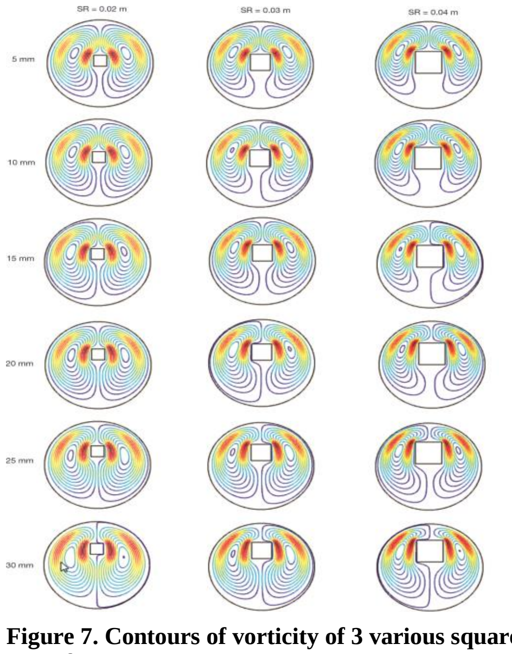

Figure 7. Contours of vorticity of 3 various square ribs of trough (SR = 0.02 m, 0.03 m, and 0.04 m) at T_w = 60 °C and p_{op} = 101 kPa for different vertical elevation of the trough (5 mm, 10 mm, 15 mm, 20 mm, 25 mm, and 30 mm)

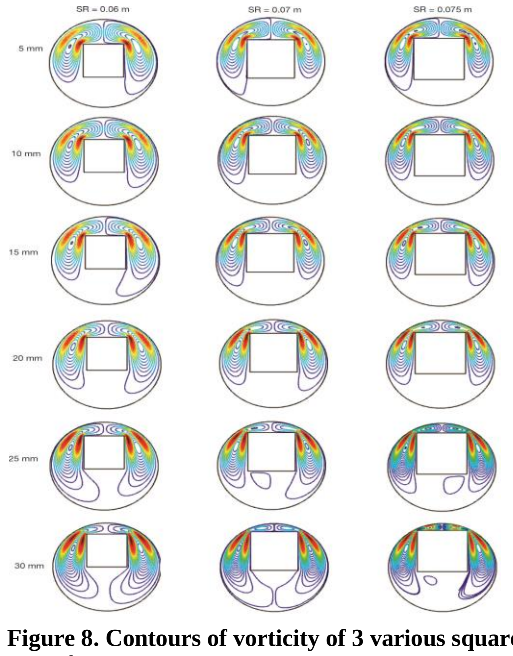

Figure 8. Contours of vorticity of 3 various square ribs of trough (SR = 0.06 m, 0.07 m, and 0.075 m) at T_w = 60 °C and p_{op} = 101 kPa for different vertical elevation of the trough (5 mm, 10 mm, 15 mm, 20 mm, 25 mm, and 30 mm)

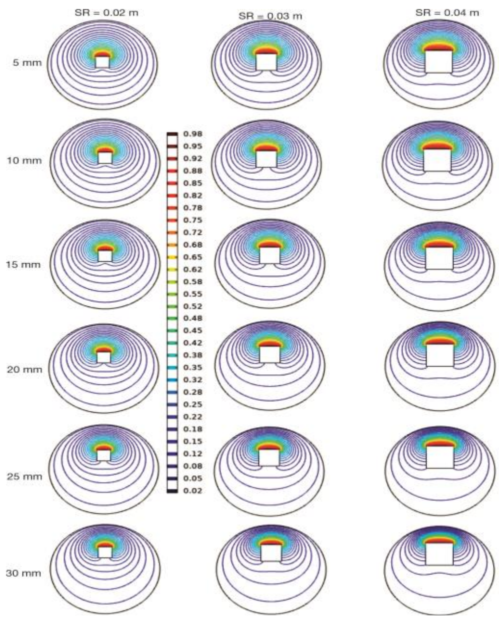

Figure 9. Contours of temperature of 3 various square ribs of trough (SR = 0.02 m, 0.03 m, and 0.04 m) at T_w = 60°C and p_{op} = 101 kPa for different vertical elevation of the trough (5 mm, 10 mm, 15 mm, 20 mm, 25 mm, and 30 mm)

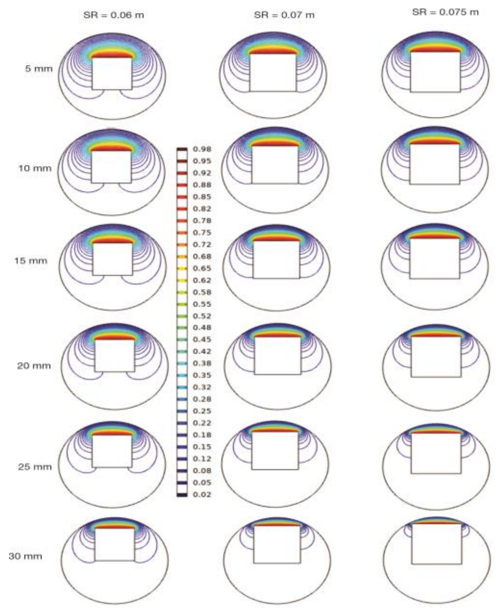

Figure 10. Contours of temperature of 3 various square ribs of trough (SR = 0.06 m, 0.07 m, and 0.075 m) at T_w = 60 °C and p_{op} = 101 kPa for different vertical elevation of the trough (5 mm, 10 mm, 15 mm, 20 mm, 25 mm, and 30 mm)

Figures 9 and 10 show the contours of temperature for several ribs of the trough (SR = 0.02 m, 0.03 m, 0.04 m, 0.05 m, 0.06 m, 0.07 m, and 0.075 m) at T_w = 60 °C and p_{op} = 101 kPa for different vertical elevation of the trough (5 mm, 10 mm, 15 mm, 20 mm, 25 mm, and 30 mm). The hot zone is clearly defined between the upper face of the square trough and the upper surface of the tubular shell in these figures. This is due to the evaporation process of the seawater. The lower area is cold because it is where purified water is recovered after condensation.

In order to investigate the influence of heat and mass transfer, we plot the Nusselt number for each square rib of the trough (20 mm, 30 mm, 40 mm, 50 mm, 60 mm, 70 mm, and 75 mm) according to the vertical elevation of the trough (5 mm, 10 mm, 15 mm, 20 mm, 25 mm, and 30 mm) at T_w = 60 °C and p_{op} = 101 kPa shown in fig. 10(a). As shown in this figure, the Nusselt number increases when the vertical elevation of the trough increases. Indeed, when the square trough is placed 30 mm to the middle of the tubular shell, the Nusselt number are 1.4243, 1.8285, 2.3423, 3.0885, 4.3166, 6.8890, and 9.9674 for the case of the rib of the square trough are 20 mm, 30 mm, 40 mm, 50 mm, 60 mm, 70 mm, and 75 mm, respectively. This increase of the Nusselt number represents respectively 12.88%, 21%, 32.93%, 51.05%, 81.14%, 145%, and 223.83% compared to the Nusselt number calculated when the trough is positioned in the middle of the tubular shell. So, we can deduce that the phenomenon of convection becomes more important with the vertical elevation of the trough. This is explained by the shrinking of the distance between the hot and cold zones as the trough dimension increases, allowing for more significant convective transfer.

To examine the influence of the distillation rate *i.e.* the productivity of distillate water of the TSS with a square trough, we plot the distillation rate for each square rib of the trough (20 mm, 30 mm, 40 mm, 50 mm, 60 mm, 70 mm, and 75 mm) according to the vertical elevation of the trough (5 mm, 10 mm, 15 mm, 20 mm, 25 mm, and 30 mm) at T_w = 60 °C and p_{op} = 101 kPa shown in fig. 11. From this figure, we observe that the productivity of distillate water increases with the increase of the vertical elevation of the trough.

Indeed, when the square trough is placed 30 mm to the middle of the tubular shell, the distillation rate are 0.23593, 0.30287, 0.38799, 0.51158, 0.71501, 1.1411, and 1.6510 kg/m^{2}hr for the case of the rib of the square trough are 20 mm, 30 mm, 40 mm, 50 mm, 60 mm, 70 mm, and 75 mm, respectively. This increase of the distillation rate represents respectively 12.88%, 21%, 32.93%, 51.05%, 81.14%, 145%, and 223.83% compared to the distillation rate calculated when the trough is positioned in the middle of the tubular shell. These percentages confirm the effect of convection and the Nusselt number seen in fig. 11. We conclude that the vertical elevation of the square trough is an essential factor for increasing the productivity of distillate water.

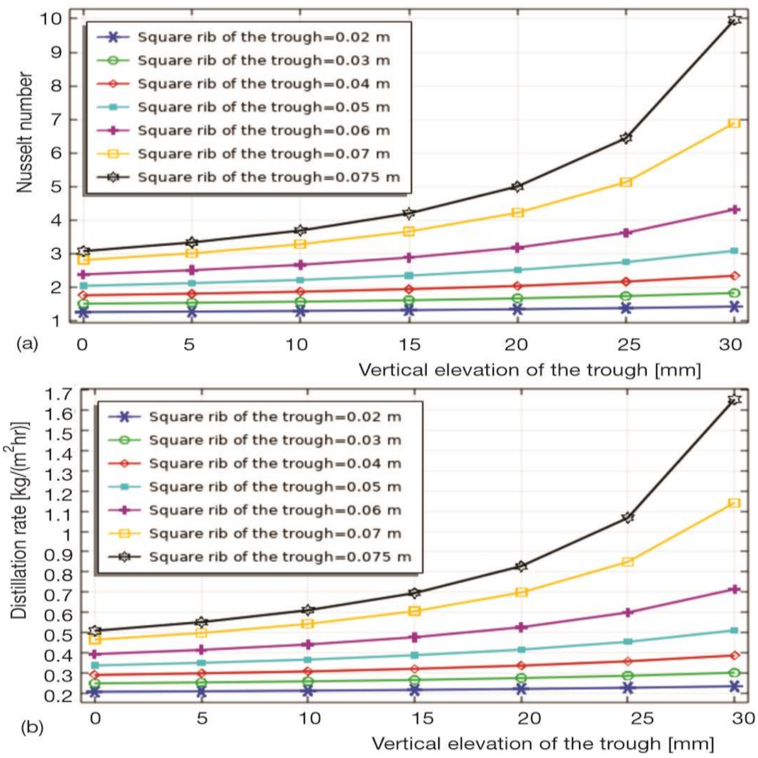

Figure 11. Evolution of (a) Nusselt number and (b) distillation rate according to the vertical elevation of the trough for different square rib at T_w = 60 °C and p_{op} = 101 kPa

Conclusion

The purpose of this research is to see if the TSS with rectangular trough can produce more distillate water by varying trough parameters. A numerical code and several simulations using Comsol Multiphysics were performed to examine the influence of the dimensions and the vertical elevation of the trough on the productivity of the water. The important findings are as follows.

- The productivity of distillate water is significantly increased with the increase of the dimensions of the trough. Compared to a rib trough of 20 mm, this quantity increase of 19,78%, 39,65%, 62%, 88.87%, 122.88%, and 144% when the rib of the square trough becomes 30 mm, 40 mm, 50 mm, 60 mm, 70 mm, and 75 mm, respectively.
- The productivity of distillate water usually increases as the vertical elevation of the trough increases from 5 mm to 30 mm. Indeed, when the square trough is placed 30 mm to the middle of the tubular shell, the distillation rate increases of 12.88%, 21%, 32.93%, 51.05%, 81.14%, 145%, and 223.83% respectively for the case of the rib of the square trough are 20 mm, 30 mm, 40 mm, 50 mm, 60 mm, 70 mm, and 75 mm, compared to the distillation rate calculated when the trough is positioned in the middle of the tubular shell.

Acknowledgement

This research has been funded by Scientific Research Deanship at University of Ha'il - Saudi Arabia through project number RG-20051.

Nomenclature

A – area, [m^2]
Br – buoyancy ratio
C – dimensionless concentration
c – concentration, [kgm^{-3}]
D_{AB} – mass diffusion coefficient, [m^{2}s^{-1}]
d_i – diffusion volume, [cm^{3}mol^{-1}]
g – acceleration of gravity, [ms^{-2}]
L_c – characteristic length (average distance between the evaporation and condensation surfaces), [m]
Le – Lewis number
L_w – width of water surface, [m]
M – molar mass, [kgmol^{-1}]
m_{hourly} – distillation rate, kg.m−2.hr−1
Nu –Nusselt number
P – dimensionless pressure
Pr – Prandtl number
p_{op} – operating pressure, [kPa]
p – pressure, [kPa]
R – radius of outer tube (tubular shell), [m]
Ra_T – thermal Rayleigh number
T – temperature, [°C]
t – time, [s]
U, V – dimensionless velocity components
u, v – velocity components in x-, y-directions, [ms^{-1}]
X, Y – dimensionless coordinate directions
x, y – co-ordinate directions, [m]

Greek symbols

α – thermal diffusivity, [m^{2}s^{-1}]
β_c – coefficient of concentration expansion, [m^{3}kg^{-1}]
β_T – coefficient of thermal expansion, [K^{-1}]
θ – dimensionless temperature
λ – thermal conductivity, [Wm^{-1}K^{-1}]
ν – kinematic viscosity, [m^{2}s^{-1}]
ρ – density, [kgm^{-3}]
τ – dimensionless time

Subscripts

A – component A in a binary diffusion system
a – air
w – water
s – surface

References

[1] Ahmed, M. Z., *et al*., Elashmawy, Basin And Tubular Solar Distillation Systems: A Review, *Process Safety and Environmental Protection, 150* (2021), June, pp. 157-178
[2] Boukhriss, M., *et al*., Simulation and Experimental Study of an AGMD Membrane Distillation Pilot for the Desalination of Seawater or Brackish Water with Zero Liquid Discharged, *Heat and Mass Transfer, 54* (2018), May, pp. 3521-3531
[3] Boukhriss, M., *et al*., The Design of a Unit Sweeping Gas Membrane Distillation: Experimental Study on a Membrane and Operating Parameters, *Applied Water Science, 10*, (2020), Apr., 110
[4] Jrad, A., *et al*., Contribution to the Study of Combined Adsorption–Ejection System Using Solar Energy, *Advances in Mechanical Engineering, 9* (2017), 7, pp. 1-9

[5] Ben Hamida, M. B., *et al*., Numerical Study of Heat and Mass Transfer Enhancement for Bubble Absorption Process of Ammonia-Water Mixture Without and With Nanofluids, *Thermal Science*, *22* (2018), 6B, pp. 3107-3120
[6] Elashmawy, M., Alshammari, F., Atmospheric Water Harvesting from Low Humid Regions Using Tubular Solar Still Powered by a Parabolic Concentrator System, *J. Clean. Prod., 256* (2020), 120329
[7] Kabeel, A. E., *et al*., Improving Performance of Tubular Solar Still by Controlling the Water Depth and Cover Cooling, *J. Clean. Prod., 233* (2019), Oct., pp. 848-856
[8] Elashmawy, M., Effect of Surface Cooling and Tube Thickness on the Performance of a High Temperature Standalone Tubular Solar Still, *Appl. Therm. Eng., 156* (2019), June, pp. 276-286
[9] Elshamy, S. M., El-Said, E. M. S., Comparative Study Based on Thermal, Exergetic and Economic Analyses of a Tubular Solar Still with Semi-Circular Corrugated Absorber, *J. Clean. Prod., 195* (2018), Sept., pp. 328-339
[10] Goshayeshi, H. R., Safaei, M. R., Effect of Absorber Plate Surface Shape and Glass Cover Inclination Angle on the Performance of a Passive Solar Still, *International Journal of Numerical Methods for Heat & Fluid Flow, 30* (2019), 6, pp. 3183-3198
[11] Arunkumar, T., *et al*., Productivity Enhancements of Compound Parabolic Concentrator Tubular Solar Stills, *Renew. Energy, 88* (2016), Apr., pp. 391-400
[12] Selvaraj, K., Natarajan, A., Factors Influencing the Performance and Productivity of Solar Stills: A Review, *Desalination, 435* (2018), June, pp. 181-187
[13] Rahbar, N., *et al*., Performance Evaluation of Two Solar Stills of Different Geometries: Tubular Versus Triangular: Experimental Study, Numerical Simulation, and Second Law Analysis, *Desalination, 443* (2018), Oct., pp. 44-55
[14] Mousa, H., *et al*., Experimental Study and Analysis of Solar Still Desalination Using Phase Change Materials, *Journal of Energy Storage, 26* (2019), 100959
[15] Vigneswaran, V. S., *et al*., Augmenting the Productivity of Solar Still Using Multiple PCMs as Heat Energy Storage, *Journal of Energy Storage, 26* (2019), 101019
[16] Ahmed, M. I., *et al*., On the Characteristics of Multistage Evacuated Solar Distillation, *Renewable Energy, 34* (2009), 6, pp. 1471-1478
[17] Gude, V. G., *et al*., Feasibility Study of a New Two-Stage Low Temperature Desalination Process, *Energy Conversion and Management, 56* (2012), Apr., pp. 192-198
[18] Xie, G., *et al*., Model Development and Experimental Verification for Tubular Solar Still Operating Under Vacuum Condition, *Energy, 157* (2018), Aug., pp. 115-130
[19] Xie, G., *et al*., Three-Effect Tubular Solar Desalination System with Vacuum Operation Under Actual Weather Conditions, *Energy Convers Manag, 205* (2020), Feb., 112371
[20] Yan, T., *et al*., CFD Investigation of Vapor Transportation in a Tubular Solar Still Operating Under Vacuum, *International Journal of Heat and Mass Transfer, 156* (2020), 119917
[21] Massaoudi, M. D., Ben Hamida, M. B., MHD Natural Convection and Thermal Radiation of Diamond–Water Nanofluid Around Rotating Elliptical Baffle Inside Inclined Trapezoidal Cavity, *The European Physical Journal Plus. 135* (2020), Nov., pp. 1-24
[22] Talukdar, P., *Et Al*., Combined Heat and Mass Transfer for Laminar Flow of Moist Air in a 3D Rectangular Duct: CFD Simulation and Validation with Experimental Data, *Int. J. Heat Mass Transf., 51* (2008), 11-12, pp. 3091-3102
[23] Fuller, E. N., *et al*., New Method for Prediction of Binary Gas-Phase Diffusion Coefficients, *Ind. Eng. Chem., 58* (1966), 5, pp. 18-27
[24] Elashmawy, M., An Experimental Investigation of a Parabolic Concentrator Solar Tracking System Integrated With a Tubular Solar Still, *Desalination, 411* (2017), June, pp. 1-4

Paper submitted: November 16, 2021
Paper revised: January 30, 2022
Paper accepted: February 1, 2022